Eur. Phys. J. D (2016) 70: 97
DOI: 10.1140/epjd/e2016-70068-x

THE EUROPEAN PHYSICAL JOURNAL D

Regular Article

The hyperfine excitation of OH radicals by He*

Sarantos Marinakis[1,a], Yulia Kalugina[2,3], and François Lique[2]

[1] Department of Chemistry and Biochemistry, School of Biological and Chemical Sciences, Queen Mary University of London, Joseph Priestley Building, Mile End Road, London E1 4NS, UK
[2] LOMC – UMR 6294, CNRS-Université du Havre, 25 rue Philippe Lebon, BP 1123, 76063, Le Havre, France
[3] Tomsk State University, 36 Lenin av., 634050 Tomsk, Russia

Received 2 February 2016 / Received in final form 3 March 2016
Published online 21 April 2016

Abstract. Hyperfine-resolved collisions between OH radicals and He atoms are investigated using quantum scattering calculations and the most recent ab initio potential energy surface, which explicitly takes into account the OH vibrational motion. Such collisions play an important role in astrophysics, in particular in the modelling of OH masers. The hyperfine-resolved collision cross sections are calculated for collision energies up to 2500 cm^{-1} from the nuclear spin free scattering S-matrices using a recoupling technique. The collisional hyperfine propensities observed are discussed. As expected, the results from our work suggest that there is a propensity for collisions with $\Delta F = \Delta j$. The new OH−He hyperfine cross sections are expected to significantly help in the modelling of OH masers from current and future astronomical observations.

1 Introduction

The most abundant nuclear constituents of interstellar molecules are H, C, O and N. Among these are the ^{14}N and ^{1}H nuclei which both have a non-zero nuclear spin with $I = 1$ and $I = 1/2$, respectively. Due to the non-zero nuclear spin, nuclear hyperfine splitting occurs in the rotational spectrum of molecules containing these nuclei, such as CN, HCN, NH_3 or OH. The hyperfine splitting is generally very small but it is well resolved in various emission spectra from molecular clouds, in particular from cold dense molecular clouds [1].

Resolving the hyperfine structure of a rotational transition is extremely useful. By assuming that all components have the same line width and excitation temperature[1], a simultaneous fit of all hyperfine components can be performed. The abundance of the molecule can be directly derived from the fit (e.g. [2]).

However, the simultaneous fit fails in several circumstances, suggesting different line widths or excitation temperatures for each component. In such cases, the hyperfine spectrum can only be interpreted through detailed radiative transfer calculations, which requires the knowledge of the hyperfine selective collisional rate coefficients, as well as hyperfine radiative rates. Radiative transfer is also necessary in the presence of hyperfine "anomalies", usually attributed to line overlap effects ([3], and references therein). Therefore a comprehensive understanding of radiative and collisional effects is crucial to interpreting molecular hyperfine spectra.

Among the interstellar molecules that possess a hyperfine structure, the OH radical is of particular significance. This is due to its high abundance in interstellar gas clouds. Since it was first discovered in the interstellar medium (ISM) by means of its radio spectrum by Weinreb et al. [4], OH has been widely observed in interstellar medium through its rotational and Λ-doublet transitions. Most recently, the Herschel Space Observatory has managed to collect many new OH emission data from young stellar objects [5], protoplanetary disks [6] and from low- and intermediate-mass protostars [7].

In addition, comprehensive models of the gas phase chemistry of diffuse interstellar clouds have revealed the importance of the OH radical in the network of reactions leading to the formation of oxygen-bearing molecules [8]. Finally, the OH radical are key species in the water chemistry network of star-forming regions, as its presence has a strong connection to the formation and destruction of water [9].

* Contribution to the Topical Issue "Atomic Cluster Collisions (7th International Symposium)", edited by Gerardo Delgado Barrio, Andrey Solov'Yov, Pablo Villarreal, Rita Prosmiti.

[a] e-mail: s.marinakis@qmul.ac.uk

[1] The excitation temperature is defined between two levels such that the Boltzmann factor, at the excitation temperature, times the ratio of the statistical weights yields the observed ratio of the population.

It is therefore crucial to have an accurate knowledge of the OH excitation conditions due to collisions with the most abundant species in interstellar clouds. In the cold ISM, the predominant collisional partner are the He atom and the molecular hydrogen [10].

Calculations of the inelastic rate coefficients for OH molecules are a complex task because OH is an open-shell species in its $^2\Pi$ ground electronic state. Despite this difficulty, the OH−H_2 system has been thoroughly studied [11,12]. Rotational, fine and hyperfine structure excitation rate coefficients in collisions with para and ortho-H_2 were provided some time ago. These values are still considered as state of the art and can be compared satisfactorily to experimental studies.

The OH(X)-He collisional system has been the object of detailed and extensive theoretical and experimental work. We refer the reader to reference [13] for a short review of previous work. OH−He fine structure-resolved rate coefficients were computed some time ago [14]. The calculations were performed using the Close Coupling approach and were based on potential energy surfaces (PES) computed by Lee et al. [15]. The OH−He calculations were validated by a detailed comparison with the crossed beam experiments of references [16,17]. More recently, a new set of three-dimensional PES for the OH($X^2\Pi$)−He van der Waals system was computed [13] (hereafter Paper I), which explicitly takes into account the OH vibrational motion. Fine structure resolved cross sections and rate coefficients were provided. The rotational cross sections and rate coefficients, which were presented in Paper I, offered an excellent agreement with experimental data ever collected, showing the high quality of the PES and of the scattering approach. This PES is also the only one used so far to reproduce OH($X^2\Pi, v = 1$) + He experimental results successfully. However, the hyperfine structure of the OH target was neglected.

Hence, we present in this paper, an extension of the calculations of Paper I to the hyperfine levels of OH at various collision energies. The paper is organized as follows: after an outline of the computational details in Section 2, the collisional cross sections are presented in Section 3. Conclusions of this work are drawn in Section 4.

2 Computational methodology

2.1 OH−He potential energy surface

For low-energy rotational excitation, we employ a new set of three-dimensional potential energy surfaces (PES) for the OH($X^2\Pi$)−He van der Waals system, which explicitly takes into account the OH vibrational motion. Ab initio calculations of the OH−He PES were carried out using the open-shell single- and double-excitation coupled cluster approach with non-iterative perturbational treatment of triple excitations [RCCSD(T)] [18,19]. The augmented correlation-consistent aug-cc-pVXZ (X = Q, 5, 6) basis sets [20] were employed, and the energies obtained were then extrapolated to the complete basis set (CBS) limit. Details of computations and plots of the PES are given in Paper I. Integral and differential cross sections (ICS and DCS), as well as thermal rate constants for the rotational excitation in OH−He collisions were calculated using the new PES, and compared with available experimental results. Experimental and theoretical results were found to be in a very good agreement. The newly constructed PES reproduces the available experimental results for OH($X^2\Pi, v = 0, 1$)−He collisions better than the previously available two-dimensional PESs, which were constructed using a fixed OH bond distance.

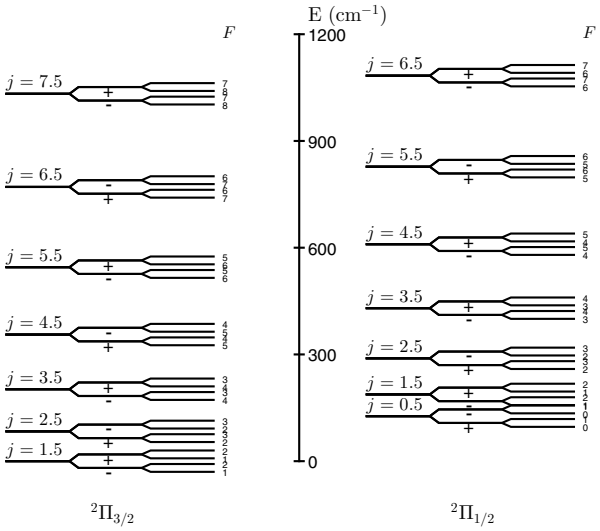

Fig. 1. Schematic representation of the lowest 56 hyperfine levels of $^{16}O^1H$. The zero reference energy is defined for the lowest OH rotational level ($\Omega = 1.5$, $j = 1.5$). The rotational levels are drawn to scale but the Λ-doubling and the hyperfine splitting are not shown to scale for clarity reasons. Note the change in ordering of the hyperfine levels for $j > 2.5$ in the $^2\Pi_{3/2}$ state, and of the Λ-doublets for $j > 3.5$ in the $^2\Pi_{1/2}$ state [22].

2.2 Scattering calculations

The main goal of this work is the use of the new OH−He PES to determine hyperfine state-resolved excitation and de-excitation integral cross sections of OH molecules by He.

The open-shell OH molecule in its ground $X\,^2\Pi$ electronic state is split into a lower (labelled F_1) and upper (F_2) spin-orbit manifold [21]. In Hund's case (a), these correspond for a molecule with a negative spin-orbit constant − as OH − to projection quantum numbers of the sum of the electronic orbital and spin angular momenta $\Omega = 3/2$ and $\Omega = 1/2$, respectively. Each rotational level j is further split into two, close-lying Λ-doublet levels, which are labelled e and f. In addition, the hydrogen atom also possesses a non-zero nuclear spin ($I = 1/2$). The coupling between $\boldsymbol{I}$ and $\boldsymbol{j}$ results in a splitting of each level into two hyperfine levels (Fig. 1). Each hyperfine level is designated by a quantum number F ($\boldsymbol{F} = \boldsymbol{I} + \boldsymbol{j}$) varying between $|I - j|$ and $I + j$.

In Paper I, we used Alexander's description [23] of the inelastic scattering between an atom and a diatomic molecule in a $^2\Pi$ electronic state and a fully-quantum close-coupling approach in order to obtain the nuclear spin free $S^J(F_i j\varepsilon l; F_i' j'\varepsilon' l')$ scattering matrices between fine structure levels of OH. J and l denote the total angular momentum ($\boldsymbol{J} = \boldsymbol{j} + \boldsymbol{l}$) and the orbital angular momentum quantum numbers, respectively, and $\varepsilon, \varepsilon'$ can be either e or f. In the calculation, the OH rotation, spin-orbit coupling and Λ-doublet splitting were taken into account, using for $v = 0$ the OH rotation constant $B = 18.5487$ cm^{-1}, the spin-orbit coupling constant $A = -139.21$ cm^{-1}, and Λ-doubling parameters $p = 0.235$ cm^{-1} and $q = -0.0391$ cm^{-1} [24]. The newly constructed PES, which takes into account the stretching of the OH molecule, was averaged using the following formula:

$$V_v(R,\theta) = \langle v(r)|V(R,\theta,r)|v(r)\rangle \tag{1}$$

where the OH vibrational wave function $|v(r)\rangle$ was evaluated using discrete variable representation (DVR) method from ab initio calculations of the OH potential function (see Paper I). All the 2D scattering calculations were performed with the HIBRIDON package [25].

The hyperfine splitting of the OH levels is extremely small. In the scattering calculations, we assume that the hyperfine levels are degenerate. Hence, it is possible to simplify considerably the hyperfine scattering problem. The integral cross sections corresponding to transitions between hyperfine levels of the OH molecule can then be obtained from scattering S-matrices between fine structure levels using the recoupling method of reference [23]. The inelastic cross sections associated with a transition from an initial hyperfine level $F_i j\varepsilon F$ to a hyperfine level $F_i' j'\varepsilon' F'$ can be obtained using the following methodology:

The total angular momentum J_T of the colliding system including nuclear spin is given by:

$$J_T = J + I. \tag{2}$$

In the recoupling scheme [26], inelastic cross sections were obtained as follows:

$$\begin{aligned}\sigma_{F_i j\varepsilon F\to F_i' j'\varepsilon' F'} = {} & \frac{\pi}{k^2_{F_i j\varepsilon F}}(2F'+1)\sum_{J_T}(2J_T+1)\\ & \times\sum_{ll'}|\delta_{F_iF_i'}\delta_{jj'}\delta_{ll'}\delta_{FF'}\\ & - S^{J_T}(F_i j\varepsilon F l; F_i' j'\varepsilon' F' l')|^2\end{aligned} \tag{3}$$

where

$$S^{J_T}(F_i j\varepsilon F l; F_i' j'\varepsilon' F' l')$$

denotes the S-matrix for a total angular momentum J_T and $k^2_{F_i j\varepsilon F}$ is the initial wavevector.

The transformation between the S^{J_T}-matrix elements and the nuclear spin-free S^J-matrix is given by:

$$\begin{aligned}S^{J_T}(F_i j\varepsilon F l; F_i' j'\varepsilon' F' l') = {} & \sum_J\left[(2F+1)(2F'+1)\right]^{1/2}(2J+1)\\ & \times(-1)^{F+F'+l+l'-2J_T}\begin{Bmatrix} l & j & J\\ I & J_T & F\end{Bmatrix}\\ & \times\begin{Bmatrix} l' & j' & J\\ I & J_T & F'\end{Bmatrix}S^J(F_i j\varepsilon l; F_i' j'\varepsilon' l').\end{aligned} \tag{4}$$

Full-quantum, close-coupling calculations were carried out on a grid of energies up to a total energy of 2500 cm^{-1}. The energy steps were 1 cm^{-1} below 1000 cm^{-1}, 5 cm^{-1} between 1000 and 1100 cm^{-1}, 10 cm^{-1} between 1100 and 1300 cm^{-1}, 25 cm^{-1} between 1300 cm^{-1} and 1800 cm^{-1}, and 50 cm^{-1} between 1800 and 2500 cm^{-1}. Calculations details to generate the nuclear spin free $S^J(F_i j\varepsilon l; F_i' j'\varepsilon' l')$ scattering matrices can be found in Paper I.

3 Results and discussions

State-to-state hyperfine cross sections for collisions of OH($^2\Pi_{3/2}, v = 0, j = 1.5e, F = 1$) and He are shown in Figures 2 and 3. At low collision energies numerous sharp spikes appear. These are a consequence of the attractive potential well in the PES. Quasi-bound states may arise from tunneling through the centrifugal energy barrier (shape resonances) or from excitation of the He−OH complex to a bend-stretch level which is energetically accessible because of the attractive well but is asymptotically closed (Feshbach resonances). The analysis of resonances is beyond the scope of this work. The cross sections for spin-orbit conserving transitions are significantly larger than those for spin-orbit changing collisions. This is in agreement with numerous previous studies of rotational cross sections in OH(X) + He [14,27–29]. This spin-orbit propensity is not as important as in other systems such as NO(X) + He [30,31]. One can clearly see that there is a strong propensity in favor of $\Delta j = \Delta F$ transitions for spin-orbit conserving transitions. This trend is the usual trend observed in hyperfine resolved collisions [23,32,33].

Hyperfine-resolved cross sections for transitions between the two lowest Λ-doublets in the lowest spin-orbit state are shown in Figure 4. All these four hyperfine transitions show maser action [34]. If one assumes a statistical model [35], then the hyperfine cross sections would be proportional to the degeneracy final state $(2F'+1)$. This is not what we observe from our calculations. Indeed, the magnitude of the collisional cross sections is governed by both the degeneracy of the final state and the coupling of the two levels. Having said that, all things being equal, the cross sections increase somewhat with an increase in F. For example, the $F = 2 \to F' = 2$ exhibits higher cross section than the $F = 1 \to F' = 1$. The most important factor, however, is the ΔF. Indeed, on the average the

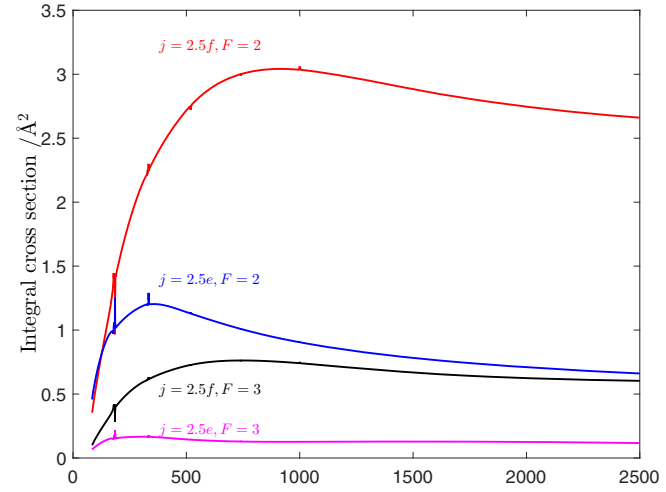

Fig. 2. State-to-state hyperfine cross sections for collisions of OH(X $^2\Pi_{3/2}, v = 0, j = 1.5e, F = 1$) and He. The results for final levels in the $j = 2.5$ for spin-orbit conserving collisions are shown. The final j, ε, F are shown in the graph.

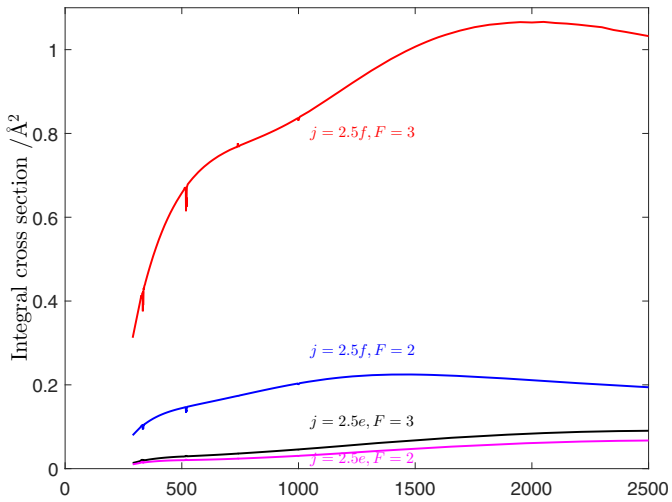

Fig. 3. State-to-state hyperfine cross sections for collisions of OH(X $^2\Pi_{3/2}, v = 0, j = 1.5e, F = 1$) and He. The results for final levels in the $j = 2.5$ for spin-orbit changing collisions are shown. The final j, ε, F are shown in the graph.

hyperfine cross sections for $\Delta F = 0$ are around 6 times higher than those for $|\Delta F| = 1$.

Similar observations are made in examining hyperfine-resolved transitions among higher Λ-doublet levels. As shown in Figure 5, for the hyperfine transitions between the higher, $j = 2.5$, Λ-doublet levels, the ratio between $\Delta F = 0$ and $|\Delta F| = 1$ cross sections is around 5 depending on the collision energy. As Corey and Alexander mentioned in their study on OH-H_2 collisions [26], the propensity for $\Delta F = 0$ is coming again from the more general collisional propensity for $\Delta F = \Delta j$ and from the tendency for preservation of the j vector. We remind that because the interaction potential is purely electrostatic in origin, and because of the absence of magnetic effects, a collision cannot affect the orientation of the I vector [26].

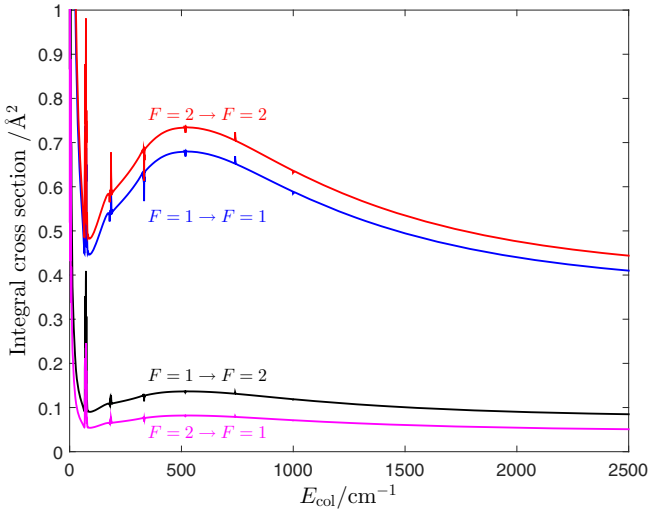

Fig. 4. State-to-state hyperfine cross sections for spin-orbit conserving collisions of OH(X $^2\Pi_{3/2}, v = 0$) and He. The initial and final levels are $j = 1.5f$ and $j = 1.5e$, respectively. The initial and final F quantum numbers are shown in the graph.

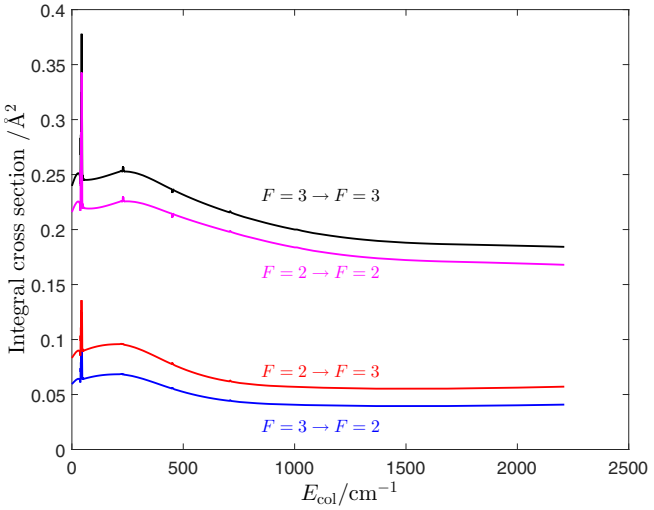

Fig. 5. State-to-state hyperfine cross sections for spin-orbit conserving collisions of OH(X $^2\Pi_{3/2}, v = 0$) and He. The initial and final levels are $j = 2.5f$ and $j = 2.5e$, respectively. The initial and final F quantum numbers are shown in the graph.

Therefore, the relative orientation of j and I, and thus the magnitude of the resultant F vector will be preserved. Our findings are in agreement with Offer et al. [12] in their study of collisions of OH with H_2.

Similar observations are also made in the spin-orbit conserving transitions in the upper spin-orbit manifold. Cross sections for transitions between the $j = 0.5$ (note that the transition $F = 0 \rightarrow F = 0$ is forbidden) and $j = 1.5$ Λ-doublet levels are shown in Figures 6 and 7.

We are now in position to examine the rotational dependence of propensities in hyperfine cross sections for transitions within a Λ-doublet. Let us assume that

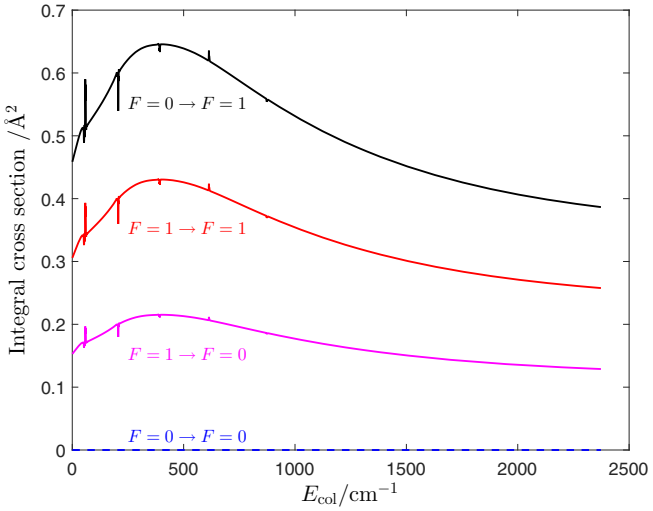

Fig. 6. State-to-state hyperfine cross sections for spin-orbit conserving collisions of OH(X $^2\Pi_{1/2}, v = 0$) and He. The initial and final levels are $j = 0.5f$ and $j = 0.5e$, respectively. The initial and final F quantum numbers are shown in the graph.

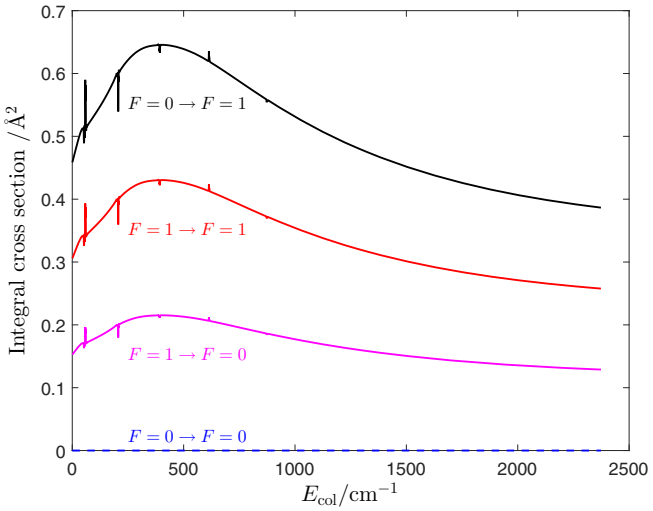

Fig. 7. State-to-state hyperfine cross sections for spin-orbit conserving collisions of OH(X $^2\Pi_{1/2}, v = 0$) and He. The initial and final levels are $j = 1.5f$ and $j = 1.5e$, respectively. The initial and final F quantum numbers are shown in the graph.

the hyperfine quantum numbers for each Λ-doublet level are $F_{\max}$ and $F_{\min}$, with $F_{\max} > F_{\min}$. The energy order will not matter in our discussion because the energy difference between these two hyperfine levels is negligible. We have four possible transitions: $F_{\max} \rightarrow F_{\max}$, $F_{\max} \rightarrow F_{\min}$, $F_{\min} \rightarrow F_{\max}$ and $F_{\min} \rightarrow F_{\min}$. The largest hyperfine cross sections will be for the transitions that $\Delta F = 0$, which are the $F_{\max} \rightarrow F_{\max}$ and $F_{\min} \rightarrow F_{\min}$. Among these two, the $F_{\max} \rightarrow F_{\max}$ will have larger cross sections because the final hyperfine quantum number is larger. Using the same argument for the $\Delta F = 1$ transitions, the smallest cross section will be for the $F_{\max} \rightarrow F_{\min}$ transition. Therefore, the cross sections

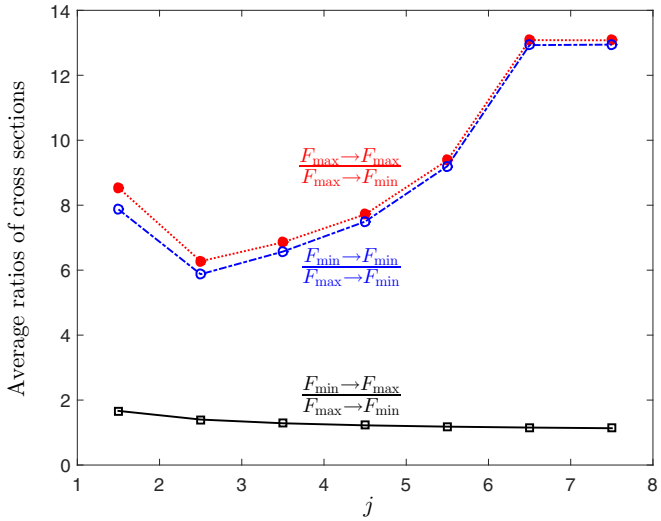

Fig. 8. Comparison of the ratios of average cross sections of $F_{\max} \rightarrow F_{\max}$ (filled red circles), $F_{\min} \rightarrow F_{\min}$ (empty blue circles), and $F_{\min} \rightarrow F_{\max}$ (black squares) over those of $F_{\max} \rightarrow F_{\min}$ as a function of j in $^2\Pi_{3/2}$.

will be larger in the following order: $F_{\max} \rightarrow F_{\max} \geq F_{\min} \rightarrow F_{\min} > F_{\min} \rightarrow F_{\max} \geq F_{\max} \rightarrow F_{\min}$. In order to directly compare these cross sections, we calculated the averages of the cross sections over the collision energy for $F_{\max} \rightarrow F_{\max}, F_{\min} \rightarrow F_{\min}, F_{\min} \rightarrow F_{\max}$ and $F_{\max} \rightarrow F_{\min}$ transitions. These averages are calculated over all the available collision energies and are non-thermal, that means that no assumption for a Boltzmann distribution was made.

In Figure 8, we plot the ratios of the average values of cross sections of $F_{\max} \rightarrow F_{\max}, F_{\min} \rightarrow F_{\min}$, $F_{\min} \rightarrow F_{\max}$ over the least probable transition $F_{\max} \rightarrow F_{\min}$ in the $^2\Pi_{3/2}$ spin-orbit state. We see that the $\Delta F = 0$ cross sections are significantly larger than of the $F_{\min} \rightarrow F_{\max}$. This propensity has a significant j-dependence, and takes the minimum value (around 6) at $j = 2.5$. The ratio of the $F_{\min} \rightarrow F_{\max}$ cross sections over those of $F_{\max} \rightarrow F_{\min}$ is around 1.667 at $j = 1.5$. The ratio tends to 1 for increasing j values. The same behavior is observed for the corresponding ratios in the $^2\Pi_{1/2}$ state, which are shown in Figure 9. The main difference is that the ratios of cross sections for $\Delta F = 0$ transitions over those of the least probable transition are monotonously increasing with j and thus do not pass through a minimum as in $^2\Pi_{3/2}$.

4 Conclusions

Quantum scattering calculations have been employed to obtain the hyperfine-resolved cross sections in OH($X^2\Pi$)−He collisions. The calculations are based on the most recent ab initio OH(X)-He PES, which treats explicitly the OH vibration. Using a recoupling method, hyperfine-resolved cross sections were obtained for collision energies up to 2500 cm^{-1}. For both spin-orbit conserving and spin-orbit changing collisions, a propensity

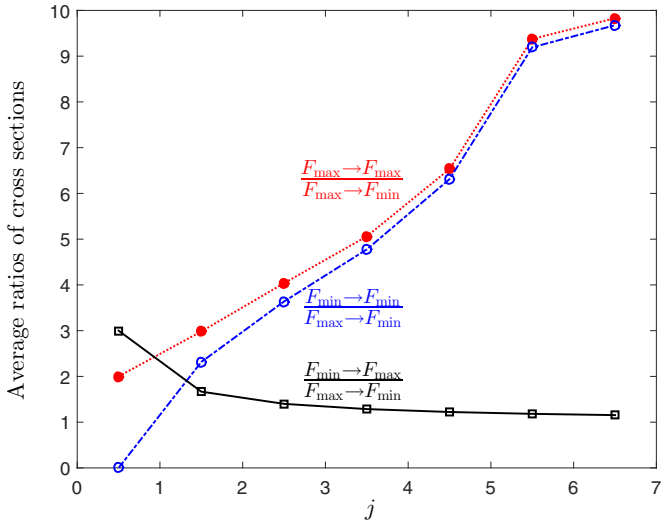

Fig. 9. Comparison of the ratios of average cross sections of $F_{max} \to F_{max}$ (filled red circles), $F_{min} \to F_{min}$ (empty blue circles), and $F_{min} \to F_{max}$ (black squares) over those of $F_{max} \to F_{min}$ as a function of j in $^2\Pi_{1/2}$.

for $\Delta F = \Delta j$ was observed. This propensity depends on the initial and final hyperfine levels and on the collision energy. Thus, a previously employed statistical model that assumed that the hyperfine cross sections are proportional to $2F'+1$, where F' is the final grand angular momentum number, should not be used. Our results, along with future calculations on OH−H_2, will shed light on the detailed mechanisms in OH masers.

Current models for the OH masers predict that radiation pumping and collisional deexcitation are responsible for $^2\Pi_{3/2}$ masers, and collisional excitation is responsible for $^2\Pi_{1/2}$ masers [34]. Collisions of OH radicals with molecular hydrogen are expected to play an important role in OH masers. In order to derive cross sections for collisions of various systems with H_2, cross sections with He are multiplied by 1.4 [36]. This approximation is a first-order estimate but cannot lead to highly accurate data. Ma et al. [37] recently obtained an ab initio PES for OH(X)−H_2. They found that OH(X)-H_2 looks more like OH(X)−Ne than OH(X)−He, and the OH−H_2 minimum is around 3 times deeper than in the OH(X)−He. This new PES was successfully tested for the study of OH(X)−H_2 rotationally-resolved collisions [38]. The extension of that work to OH(X)−H_2 hyperfine-resolved collisions will provide an important test for the current models for OH masers. Such theoretical treatment can be applied to other $^2\Pi$ radicals that have hyperfine structure such as CH and NO for which collisional data are crucially needed to analyse astronomical spectra.

S.M. and F.L. greatly acknowledge the financial support of ANR project "HYDRIDES". This work was supported by the CNRS program "Physique et Chimie du Milieu Interstellaire" (PCMI). Y.K. acknowledges the support of Russian Foundation for Basic Research, grant 15-05-00736 and Tomsk State University supercomputer center "SKIF-Cyberia".

References

1. F. Daniel, M. Gérin, E. Roueff, J. Cernicharo, N. Marcelino, F. Lique, D.C. Lis, D. Teyssier, N. Biver, D. Bockéele-Morvan, A&A **560**, A3 (2013)
2. M. Padovani, C.M. Walmsley, M. Tafalla, P. Hily-Blant, G. Pineau des Forêts, A&A **534**, A77 (2011)
3. R.M. Loughnane, M.P. Redman, M.A. Thompson, N. Lo, B. O'Dwyer, M.R. Cunningham, MNRAS **420**, 1367 (2012)
4. S. Weinreb, A.H. Barrett, M.L. Meeks, J.C. Henry, Nature **200**, 829 (1963)
5. S.F. Wampfler et al., A&A **521**, L36 (2010)
6. D. Fedele et al., A&A **559**, A77 (2013)
7. S.F. Wampfler et al., A&A **552**, A56 (2013)
8. S. Viti, E. Roueff, T.W. Hartquist, G. Pineau des Forêts, D.A. Williams, A&A **370**, 557 (2001)
9. E.F. van Dishoeck, E. Herbst, D.A. Neufeld, Chem. Rev. **113**, 9043 (2013)
10. E. Roueff, F. Lique, Chem. Rev. **113**, 8906 (2013)
11. D.P. Dewangan, D.R. Flower, M.H. Alexander, MNRAS **226**, 505 (1987)
12. A.R. Offer, M.C. van Hemert, E.F. van Dishoeck, J. Chem. Phys. **100**, 362 (1994)
13. Y. Kalugina, F. Lique, S. Marinakis, Phys. Chem. Chem. Phys. **16**, 13500 (2014)
14. J. Kłos, F. Lique, M.H. Alexander, Chem. Phys. Lett. **445**, 12 (2007)
15. H.S. Lee, A. McCoy, R. Toczyłowski, S. Cybulski, J. Chem. Phys. **113**, 5736 (2000)
16. K. Schreel, J. Schleipen, A. Eppink, J.J. ter Meulen, J. Chem. Phys. **99**, 8713 (1993)
17. M. Kirste, L. Scharfenberg, J. Kłos, F. Lique, M.H. Alexander, G. Meijer, S.Y.T. van de Meerakker, Phys. Rev. A **82**, 042717 (2010)
18. P.J. Knowles, C. Hampel, H.J. Werner, J. Chem. Phys. **99**, 5219 (1993)
19. P.J. Knowles, C. Hampel, H.J. Werner, J. Chem. Phys. **112**, 3106 (2000)
20. D.E. Woon, T.H. Dunning Jr., J. Chem. Phys. **100**, 2975 (1994)
21. K.P. Huber, G. Herzberg, *Molecular Spectra and Molecular Structure. IV. Constants of Diatomic Molecules* (Van Nostrand Reinhold, New York, 1979)
22. J.M. Brown, M. Kaise, C.M.L. Kerr, D.J. Milton, Mol. Phys. **36**, 553 (1978)
23. M.H. Alexander, Chem. Phys. **92**, 337 (1985)
24. J.J. Gilijamse, S. Hoekstra, S.Y.T. van de Meerakker, G.C. Groenenboom, G. Meijer, Science **313**, 1617 (2006)
25. The HIBRIDON package was written by M.H. Alexander, D.E. Manolopoulos, H.-J. Werner, B. Follmeg, with contributions by P.F. Vohralik, D. Lemoine, G. Corey, R. Gordon, B. Johnson, T. Orlikowski, A. Berning, A. Degli-Esposti, C. Rist, P. Dagdigian, B. Pouilly, G. van der Sanden, M. Yang, F. de Weerd, S. Gregurick, J. Kłos, http://www2.chem.umd.edu/groups/alexander/
26. G.C. Corey, M.H. Alexander, J. Chem. Phys. **88**, 6931 (1988)
27. L. González-Sánchez, E. Bodo, F.A. Gianturco, Phys. Rev. A **73**, 022703 (2006)

28. S. Marinakis, G. Paterson, J. Kłos, M.L. Costen, K.G. McKendrick, Phys. Chem. Chem. Phys. **9**, 4414 (2007)
29. G. Sarma, S. Marinakis, J.J. ter Meulen, D.H. Parker, K.G. McKendrick, Nat. Chem. **4**, 985 (2012)
30. F.J. Aoiz, J.E. Verdasco, M. Brouard, J. Kłos, J. Phys. Chem. A **113**, 14636 (2009)
31. L. Scharfenberg, K.B. Gubbels, M. Kirste, G.C. Groenenboom, G. Meijer, S.Y.T. van de Meerakker, Eur. Phys. J. D **65**, 189 (2011)
32. F. Lique, J. Kłos, MNRAS **413**, L20 (2011)
33. M. Lanza, F. Lique, MNRAS **424**, 1261 (2012)
34. R. Cesaroni, C.M. Walmsley, A&A **241**, A77 (1991)
35. F.A. Franz, J.R. Franz, Phys. Rev. **148**, 82 (1966)
36. F.L. Schöier, F.F.S. van der Tak, E.F. van Dishoeck, J.H. Black, A&A **432**, 369 (2005)
37. Q. Ma, J. Kłos, M.H. Alexander, A. van der Avoird, P.J. Dagdigian, J. Chem. Phys. **141**, 174309 (2014)
38. H. Christian Schewe, Q. Ma, N. Vanhaecke, X. Wang, J. Kłos, M.H. Alexander, S.Y.T. van de Meerakker, G. Meijer, A. van der Avoird, P.J. Dagdigian, J. Chem. Phys. **142**, 204310 (2015)